Supporting Information for "Radar-sounding characterization of the subglacial groundwater table beneath Hiawatha Crater, Greenland"

Jonathan T. Bessette[1,2], Dustin M. Schroeder[2,3], Thomas M. Jordan[2,4], and

Joseph A. MacGregor[5]

[1]Department of Mechanical and Aerospace Engineering, University at Buffalo, Buffalo, NY, USA

[2]Department of Geophysics, Stanford University, Stanford, CA, USA

[3]Department of Electrical Engineering, Stanford University, Stanford, CA, USA

[4]School of Geographical Sciences, University of Bristol, Bristol, UK

[5]Cryospheric Sciences Laboratory, NASA Goddard Space Flight Center, Greenbelt, Maryland, USA

Contents of this file

1. Text S1 to S4

2. Figures S1 to S3

3. Tables S1 to S2

Introduction

Text and Figure S1. Estimation of englacial attenuation

Text and Figure S2. Distributions of ice-basal layer and basal layer-subsurface reflectivities

Text and Figure S3. Relative reflectivity map of the Hiawatha Crater

———

April 17, 2021, 4:34pm

Text S1. Estimation of englacial attenuation

To estimate the relative reflectivity of the ice–basal layer and basal layer–groundwater interfaces, the englacial attenuation rate must first be calculated. Following Jacobel et al. (2009) and assuming the complex permittivity of the ice is uniform, a linear best-fit englacial attenuation rate is obtained by plotting peak power returned versus ice thickness, which is equal to half the radar path length (Fig. S1). This slope is equivalent to a depth-averaged, one-way attenuation rate of ~19 dB km^{-1}, which is roughly consistent with englacial-layer derived attenuation rates ranging from 10 dB km^{-1} in the inner regions of the Greenland Ice Sheet to greater than 25 dB km^{-1} at the ice–sheet margin (MacGregor et al., 2015) and with results of attenuation in the Hiawatha Crater region of Northwest Greenland ranging from about 15 dB km^{-1} to 30 dB km^{-1}, according to modeled values (Jordan et al., 2016).

Text S2. Distributions of ice-basal layer and basal layer-subsurface reflectivities

To characterize the impact of roughness-induced scattering loss, we compared the spread of the relative reflectivity distributions from the ice–basal layer and basal layer–groundwater interfaces (Jordan et al., 2018; Grima et al., 2019). We used the distribution of peak echo power from each reflector as a proxy for the scattering loss, assuming that

the permittivities of each material are uniform (Neal, 1982; Grima et al., 2014). We compared the bed (ice-basal layer interface) reflectivity and the groundwater table (basal layer-groundwater saturated till interface) reflectivity distributions for each segment individually. The relative reflectivity standard deviations for the ice–basal layer and basal layer–groundwater interfaces are 5.3 dB and 8.4 dB, respectively. These values are consistent with interface roughness loss having a similar effect upon each layer. We observed that the spread of the distributions for the bed reflectivities and the groundwater table reflectivities are broadly comparable (Fig. S2). Hence, our interpretation of $\Delta[R]$ assuming specular reflections is robust, because all things being equal, the bias from possible roughness-induced scattering loss is comparable for each interface. In turn, because we are interested in the difference in the interfacial reflectivities (ΔR), this result justifies that roughness can be neglected from the analysis.

Text S3. Reflectivity map of the Hiawatha Crater

S3 shows a relative reflectivity map for the ice-bed interface of the Hiawatha Crater generated from the 2016 AWI survey data. Flight segments were manually trimmed to encompass segments within the crater only. Power was geometrically corrected and attenuation loss in the ice was incorporated from S3.

Text S4. Seasonal influence on results Both models are unlikely to be affected by seasonal inputs to the bed from supraglacial melting. In their Supplementary Information, Kjær et al. (2018) mapped moulin locations on Hiawatha Glacier from meter-scale satellite imagery and found that they are located at the onset of the glacier tongue and to the northeast thereof, so surface meltwater inputs are clearly not compatible with the extent of putative groundwater table detection. It is possible that, in our first hypothesized

model, later in the melt season water could flow above the aquitard of the frozen basal layer. If this was observed, it would serve as a hypothesis test between the two models. Dedicated ground-based geophysical surveys, including seismic and resistivity sounding, could confirm our interpretations and add additional glaciological, hydrological, and geological context.

Text S5. Justification of material properties The dielectric value for groundwater-saturated till, corresponding to the bottom layer of model 1, was calculated *a posteriori* by analyzing an entire range of groundwater permittivities provided by Christianson et al. (2016). We swept this range of dielectric values, producing corresponding ternary diagrams, and identified the dielectric value for groundwater till that maximized the region of overlap within the ternary diagram. This region of overlap corresponds with where the radiometrically determined loss tangent and relative reflectivity calculations are in agreement. The dielectric value for the bottom layer of model 2 was taken directly from Christianson et al. (2016). The dielectric value of granite, which is one of the three components within the mixing model of the middle layer, was plotted on the ternary diagrams (Fig. 3) considering a range of granite compositions, i.e. sand or rock. Thus, the shaded areas correspond to a range of possible granite permittivities to mitigate uncertainty in chosen dielectric properties. The permittivity of ice chosen is the same value used by Kjær et al. (2018).

The values of density for granitic sand correspond to the values used in other studies of Greenland by Corbett, Bierman, Lasher, and Rood (2015) and Vermassen et al. (2019). While granitic sand mostly alligns with the description of model 1, we use this same density for fractured granite in the bottom layer of model 2 because similar values have

been employed for solid granite rock. We also note, the purpose of the material densities are for calculating an estimate of hydraulic potential contours and checking for reasonable agreement with the radar echoes- rather than robust hydrologic accuracy. The density of groundwater-saturated till is assumed to be equivalent to groundwater, because the till will not flow. Thus, the two hydraulic potential calculations involve using the density of water for the bottom layer - however, the permittivities of the bottom layer still differ between models.

A summary of these material properties can be found in Table S2.

Text S6. Data availability All data used is stored in CReSIS Data Products under Radar Depth Sounder Data Products, with the four segments labeled in Figure 1 by their filename in the database specific to the Greenland Polar 6 survey in 2016 (CReSIS, 2016). Specific URLs to the Matlab data for the segments a, b, c, and d in Fig. 1 are listed below.

a. in blue 20160517_03_008: `https://data.cresis.ku.edu/data/rds/2016_Greenland` `_Polar6/CSARP_standard/20160517_03/Data_20160517_03_008.mat`

b. in green 20160512_02_009: `https://data.cresis.ku.edu/data/rds/2016_Greenland` `_Polar6/CSARP_standard/20160512_02/Data_20160512_02_009.mat`

c. in orange 20160516_02_006: `https://data.cresis.ku.edu/data/rds/2016_Greenland` `_Polar6/CSARP_standard/20160516_02/Data_20160516_02_006.mat`

d. in purple 20160512_02_007: `https://data.cresis.ku.edu/data/rds/2016_Greenland` `_Polar6/CSARP_standard/20160512_02/Data_20160512_02_007.mat`

Metadata for utilizing these data products is provided by CReSIS here `https://data` `.cresis.ku.edu/data/rds/rds_readme.pdf`

References

Christianson, K., Jacobel, R. W., Horgan, H. J., Alley, R. B., Anandakrishnan, S., Holland, D. M., & DallaSanta, K. J. (2016). Basal conditions at the grounding zone of Whillans Ice Stream, West Antarctica, from ice-penetrating radar. *Journal of Geophysical Research: Earth Surface*, *121*(11), 1954-1983. doi: https://doi.org/10.1002/2015JF003806

Corbett, L. B., Bierman, P. R., Lasher, G. E., & Rood, D. H. (2015). Landscape chronology and glacial history in Thule, northwest Greenland. *Quaternary Science Reviews*, *109*, 57–67. doi: https://doi.org/10.1016/j.quascirev.2014.11.019

CReSIS. (2016). 2016 greenland polar6 data. `https://data.cresis.ku.edu/data/rds/2016_Greenland_Polar6/`.

Grima, C., Koch, I., Greenbaum, J., Soderlund, K., Blankenship, D., Young, D., . . . Fitzsimons, S. (2019). Surface and basal boundary conditions at the Southern McMurdo and Ross Ice Shelves, Antarctica. *Journal of Glaciology*, *65*(252), 675–688. doi: https://doi.org/10.1017/jog.2019.44

Jacobel, R. W., Welch, B. C., Osterhouse, D., Pettersson, R., & MacGregor, J. A. (2009). Spatial variation of radar-derived basal conditions on Kamb Ice Stream, West Antarctica. *Annals of Glaciology*, *50*(51), 10–16. doi: https://doi.org/10.3189/172756409789097504

Jordan, T. M., Bamber, J. L., Williams, C. N., Paden, J. D., Siegert, M. J., Huybrechts, P., . . . Gillet-Chaulet, F. (2016). An ice-sheet-wide framework for englacial attenuation from ice-penetrating radar data. *The Cryosphere*, *10*, 1547–1570. doi: https://doi.org/10.5194/tc-10-1547-2016

Jordan, T. M., Williams, C. N., Schroeder, D. M., Martos, Y. M., Cooper, M. A., Siegert, M. J., . . . Bamber, J. L. (2018). A constraint upon the basal water distribution and thermal state of the Greenland Ice Sheet from radar bed echoes. *Cryosphere*, *12*, 2831-2854. doi: https://doi.org/10.5194/tc-12-2831-2018

Kjær, K. H., Larsen, N. K., Binder, T., Bjørk, A. A., Eisen, O., Fahnestock, M. A., . . . MacGregor, J. A. (2018). A large impact crater beneath Hiawatha Glacier in northwest Greenland. *Science Advances*, *4*(11). doi: https://doi.org/10.1126/sciadv.aar8173

MacGregor, J. A., Li, J., Paden, J. D., Catania, G. A., Clow, G. D., Fahnestock, M. A., . . . Stillman, D. E. (2015). Radar attenuation and temperature within the Greenland Ice Sheet. *Journal of Geophysical Research: Earth Surface*, *120*(6), 983-1008. doi: https://doi.org/10.1002/2014JF003418

Vermassen, F., Wangner, D. J., Dyke, L. M., Schmidt, S., Cordua, A. E., Kjær, K. H., . . . Andresen, C. S. (2019). Evaluating ice-rafted debris as a proxy for glacier calving in Upernavik Isfjord, NW Greenland. *Journal of Quaternary Science*, *34*(3), 258–267. doi: https://doi.org/10.1002/jqs.3095
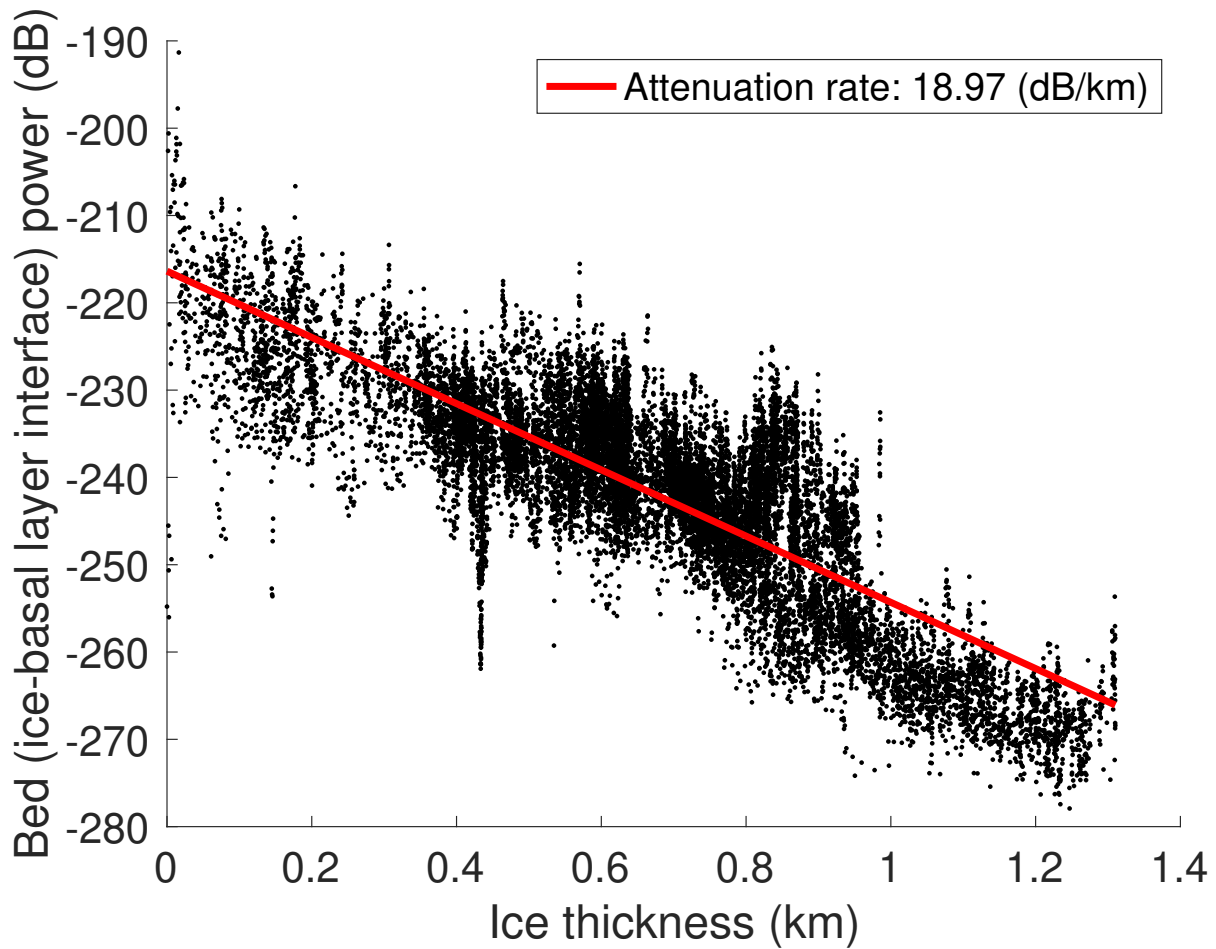
Figure S1. Bed (ice-basal layer interface) power versus ice-sheet thickness for the determination of the depth-averaged attenuation rate in ice.

Table S1. Radar system characteristics.

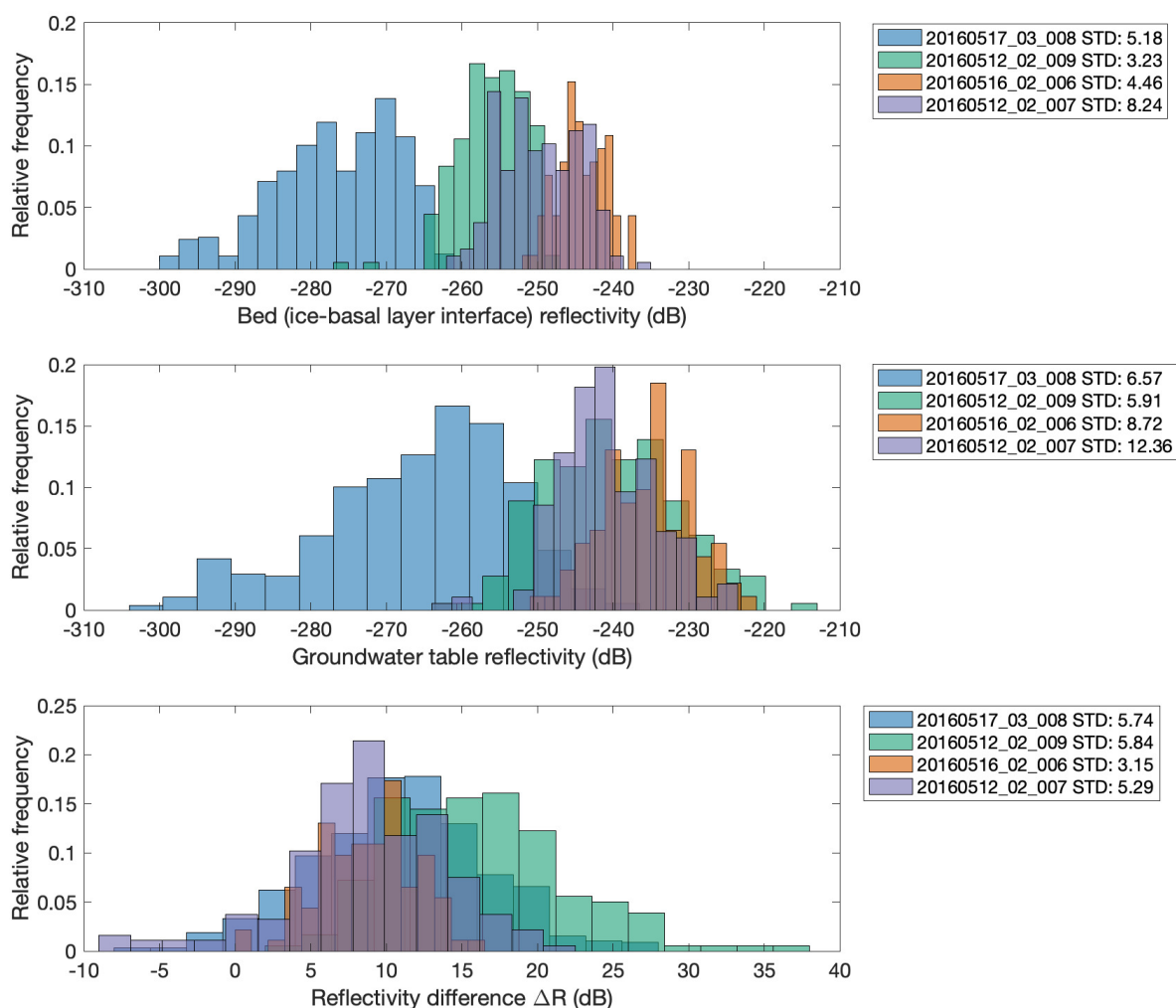| System	Bandwidth (MHz)	Center frequency (MHz)	Pulse length (μs)	Window
MCoRDS v5	370	335	3	Tukey
MCoRDS v3	30	190	10	Tukey
HiCARS	15	60	1	Hann

Figure S2. Frequency distributions for the bed (ice–basal layer interface) reflectivity, the basal layer–groundwater reflectivity, and the difference between the two reflectivities, ΔR. Each segment is labeled by it's respective data file name and the corresponding standard deviation is shown in the legend.
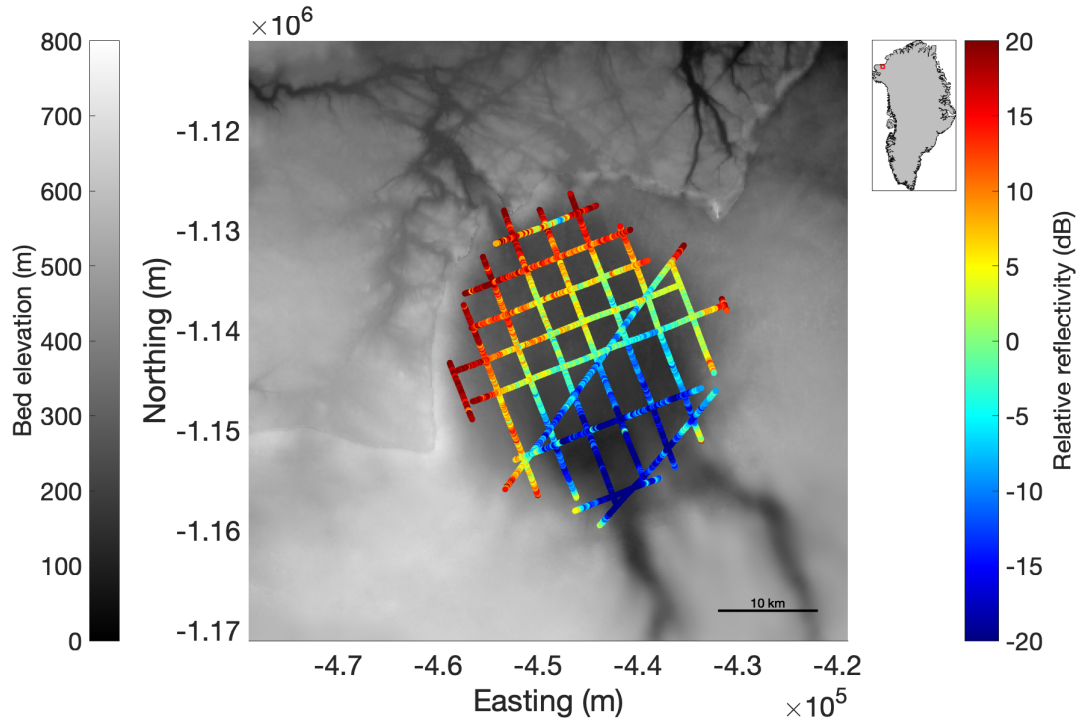
:

Figure S3. Relative reflectivity map of the Hiawatha Crater in northwest Greenland

Table S2. Assumed material dielectric properties.

Material	Density (kg m^{-3})	Complex permittivity ($\tilde{\epsilon}$)
Granite	2700	$5(1 - j6.8 \times 10^{-5}) < \tilde{\epsilon}_{gran} < 9(1 - j0.068)$
Ice	910	$3.15(1 - j0.0062)$
Groundwater-saturated till	997	$20(1 - j0.005) < \tilde{\epsilon}_{gw} < 30(1 - j0.015)$
Groundwater	997	$\tilde{\epsilon}_w = 80(1 - j0.2482)$

April 17, 2021, 4:34pm